Surface texture characterisation with reduced boundary effect for diamond-turned micro-structured surfaces

Pan Guo[a], Mingyu Liu[b], Bowen Zhang[a], Jintao Li[a], Zhiwen Xiong[a], Samanta Piano[b], Shaojian Zhang[a,*]

[a]Key Laboratory of Ultra-precision Machining Technology, School of Advanced Manufacturing, Nanchang University, Nanchang, Jiangxi, PR China.

[b]Manufacturing Metrology Team, Faculty of Engineering, University of Nottingham, Nottingham, UK.

[*] E-mail: zhangshaojian@ncu.edu.cn

Abstract

Micro-structured surfaces, fabricated by ultra-precision diamond turning (UPDT) with nanometric surface texture, have been widely used due to their wide range of functionalities. Their functional performance is closely related to their surface texture. To characterise the surface texture of the micro-structured surfaces, boundary effect would happen in the boundary area when surface filtering and yield a crucial impact upon their characterisation. However, the boundary effect has received relatively little attention for the surface texture characterisation. Hence, this study focuses on discussing the boundary effect in characterising the surface texture of micro-structured surfaces. Firstly, discrete wavelet transform (DWT) is used to extract the surface texture from the primary surface. Secondly, a probability-based approach is applied to remove the points with large amplitude at the boundary area of the micro-structures in order to reduce the boundary effect. Finally, the UPDT experiment is conducted for the fabrication of micro-structured surfaces and their surface texture is evaluated by the height parameters *Sa*, *Sq, Sz*, *Ssk*, and *Sku* of ISO 25178-2. The results show that the boundary effect can be reduced efficiently by the probability-based approach during surface filtering. Moreover, *Sz*, *Ssk*, and *Sku* could be more sensitive to the boundary effect than *Sa* and *Sq* due to their different statistical characteristics. Significantly, the study provides an effective method to reduce bound effect in characterising the surface texture of micro-structured surfaces.

Keywords: Micro-structured surfaces; Ultra-precision diamond turning; Surface texture; Boundary effect; Discrete wavelet transform

1. Introduction

Micro-structured surfaces have been widely applied in precision systems as they have a wide range of functionalities [1, 2]. Ultra-precision diamond turning (UPDT), a promising technique with high flexibility and relatively low cost [3, 4], has been commonly used for the high-quality fabrication of micro-structured surfaces which can have nanometric surface texture [5, 6]. Surface texture parameters, as important indicators, often determine the functional performances such as fatigue strength, friction behaviour, optical interference and diffraction of the machined surfaces [7, 8]. One of key issues in surface metrology is to relate the functionality of machined surface to the surface texture [9]. Pawlus et al. [10] systematically analysed the surface texture parameters, the oil capacity, and the low-wear assessment originated from the material ratio curve, the contained information on surface texture to its functional performance is well correlated from the material ratio curve. Hereby, it is critical to accurately evaluate the nanometric surface texture for micro-structured surfaces. The process for surface texture characterisation generally consists of: (1) measure the surface using surface measurement instruments such as profilometers, white light interferometers, and atomic force microscopes [11]; (2) extract the surface texture from the primary surface using areal filters [12]; (3) calculate the surface texture parameters according to ISO 25178-2 [12].

Commercial surface measurement instruments, such as white light interferometers, provide a promising surface measurement for a wide range of textured surfaces. Nieslony et al. [13] focused on characterising the surface texture of the explosively clad Ti–steel plates after drilling process, in which the stylus-based and optical profilometry were utilised for the surface measurement. The results indicated that the surface texture parameters were much dependent on the measurement methods. Moreover, efficient separation of surface texture from the primary surface is an important step for texture characterisation [14]. Gaussian filter, as a widely used filtering method, convolves the measured data with a Gaussian weighting function to obtain the filtered data [15]. The Gaussian filter has replaced the 2RC (second-order resistor-capacitor circuit) filter which has a serious phase distortion [15]. However, the Gaussian filter is insufficient to deal with surfaces with large peak-valley values and outliers with large amplitudes, as it would result in distortions for surface texture evaluation [15]. For the filtering of micro-structured surfaces, the Gaussian filter has poor

performance due to its averaging effect and large distortions can be found in the boundary areas [16]. The spline filter has also been widely applied for surface filtering. However, its applications on micro-structured surfaces filtering are limited, as it is difficult for the spline filter to retain sharp geometries which are often found in micro-structured surfaces [17]. To reduce the boundary effect, robust Gaussian filters [18] and robust spline filters [19] were introduced by integrating a robust estimating procedure. However, the robust filters have high computational complexity, which makes it difficult to be applied on surfaces with a relatively large amount of data (typically one million data points, which is a common practice in modern surface measurement instruments). One method to reduce the boundary effect is to extrapolate data outside the boundary of the measured surfaces [20], which however introduces extrapolation errors and is difficult to implement for micro-structured surfaces with complex features.

Wavelet transform has been applied for surface texture characterisation to extract the texture data from the surface topography data [21, 22]. Compared to conventional methods such as the Gaussian filter, smaller distortions in the filtered topography data can be obtained using the wavelet transform method [23]. As a result, the wavelet transform method is promising to filter surface texture with high accuracy. Zou et al. [24] applied discrete wavelet transform (DWT) to effectively extract the surface texture from a turbine blade surface. Wang et al. [25] used the wavelet transform for the surface texture characterisation of engineering surfaces. Ali et al. [26] adopted the wavelet transform to evaluate electrical discharge machined surfaces. For UPDT, Wang et al. [27] used wavelet transform to decompose surface topography and accurately assessed the nanometric surface texture for surfaces machined under different cutting conditions. The effectiveness of wavelet transform for multi-scale analysis of surface topography has been demonstrated in the literature [28]. However, the boundary effect can still be found at the boundary areas when extracting the surface texture using wavelet transform [29]. Due to the complexity of surface features in micro-structured surfaces, the boundary effect is the key issue affecting the accuracy of surface texture characterisation, as the boundary effect introduces large errors in the calculations of surface texture parameters.

Nevertheless, the boundary effect has received relatively little attention during surface filtering for the surface texture characterisation of micro-structured surfaces. To reduce the boundary effect in

texture characterisation for microstructured surfaces, we proposed a method that combines DWT and a probability-based approach. Different from the traditional operations for reducing the boundary effect, the filtered surface texture need to be manully removed at the boundary area for micro-structured surfaces, which inevitablely makes the characterisation to be incomplete and inefficient [15]. In the proposed method, DWT was conducted for the filtering of surface texture from the micro-structured surfaces, and a probability-based approach with the so-called "95-99 rule" [8] (statistically removing 5% and 1% data points for the calculations of different texture parameters) was applied to reduce the boundary effect. Comparison experiments of surface texture parameters calculated with boundary effect and with reduced boundary effect were conducted and the results showed that the proposed method is effective.

2. Theoretical model

2.1 Discrete wavelet transform

One practice, according to ISO 25178-2, to extract the surface texture from the measured surface is to apply an S-filter, an F-operation, and an L-filter [12]. To obtain the primary surface, small-scale lateral components are firstly removed by an S-filter. Next, the form component is removed from the primary surface by an F-operation to get an S-F surface. Then, the large-scale lateral components from the S-F surface are removed by applying an L-filter. After that, an S-L surface is obtained. The surface texture parameters can then be calculated based on the scale-limited surface (an S-F surface or an S-L surface). Wavelet transform can be applied in surface filtering. One-dimensional wavelet transform is commonly used for profile filtering. A family of wavelets $\psi_{u,s}(x)$ can be obtained by scaling and shifting a prototype function called the mother wavelet $\psi(x)$ [24]:

$$\psi_{u,s}(x) = \frac{1}{\sqrt{s}}\psi\left(\frac{x-u}{s}\right) \tag{1}$$

where s is the scale factor and u is the translation factor. The two-dimensional wavelet transform can be used for the areal filtering, its scaling function is modified as:

$$\varphi(x, y) = \varphi(x)\varphi(y) \tag{2}$$

where $\varphi(x)$ and $\varphi(y)$ are the scaling functions of the mother wavelet. The wavelet functions are

extended to the following:

$$\begin{aligned}\psi^H(x, y) &= \varphi(x)\psi(y)\\ \psi^V(x, y) &= \psi(x)\varphi(y)\\ \psi^D(x, y) &= \psi(x)\psi(y)\end{aligned} \tag{3}$$

where $\psi^H(x, y)$, $\psi^V(x, y)$, and $\psi^D(x, y)$ are the wavelet functions along horizontal, vertical, and diagonal directions respectively, $\psi(x)$ and $\psi(y)$ are the wavelet functions of the mother wavelet. For a surface topography $f(x, y)$ with $M \times N$ points along horizontal and vertical directions, the two-dimension DWT decomposes it into the approximate coefficient $W_\varphi(j_0, m, n)$ (the low-frequency component) and the detail coefficient $W_\psi^i(j, m, n)$ (the high-frequency component), which are:

$$\begin{cases} W_\varphi(j_0, m, n) = \dfrac{1}{\sqrt{MN}} \displaystyle\sum_{x=0}^{M-1}\sum_{y=0}^{N-1} f(x, y)\varphi_{j_0, m, n}(x, y) \\ W_\psi^i(j, m, n) = \dfrac{1}{\sqrt{MN}} \displaystyle\sum_{x=0}^{M-1}\sum_{y=0}^{N-1} f(x, y)\psi^i{}_{j, m, n}(x, y) \end{cases} \tag{4}$$

where $\varphi_{j_0, m, n}(x, y)$ is the scale function and $\psi^i{}_{j, m, n}(x, y)$ is the wavelet function, i represents the wavelet function along horizontal, vertical or diagonal directions, j_0 is the initial value for the decomposition and commonly denoted as 0. J is the decompose level and $j = 0, 1, 2, \ldots, J-1$, $M = N = 2^J$ with $m, n = 0, 1, 2, \ldots, 2^j - 1$, where m and n are the scale along horizontal and vertical directions respectively. The two-dimensional DWT is achieved by a dual channel filter which contains a low pass filter h and a high pass filter g with down-sampling, where the low pass filter and the high pass filter are realised by the scaling function and the wavelet function respectively. The decomposition begins with the approximation A_j in the level j, then undergoes the high pass filtering g and the low pass filtering h that successively take place in rows and columns, resulting a new approximation coefficient A_{j+1} with low-frequency and three detail coefficients D_{j+1}^H, D_{j+1}^V, and D_{j+1}^D with high-frequency in the next level j+1 [24]. The important information can be captured in the detail coefficients of wavelet decomposition. The above process is shown in Fig. 1, the relationship between the approximation coefficients and the detail coefficients is expressed as:

$$A_j = A_{j+1} + D_{j+1}^H + D_{j+1}^V + D_{j+1}^D \quad (5)$$

The relationship among the primary surface S, the approximate coefficients, and the detail coefficients at a selected level j is as follow:

$$S = A_j + \sum_{i=1}^{j} (D_i^H + D_i^V + D_i^D) \quad (6)$$

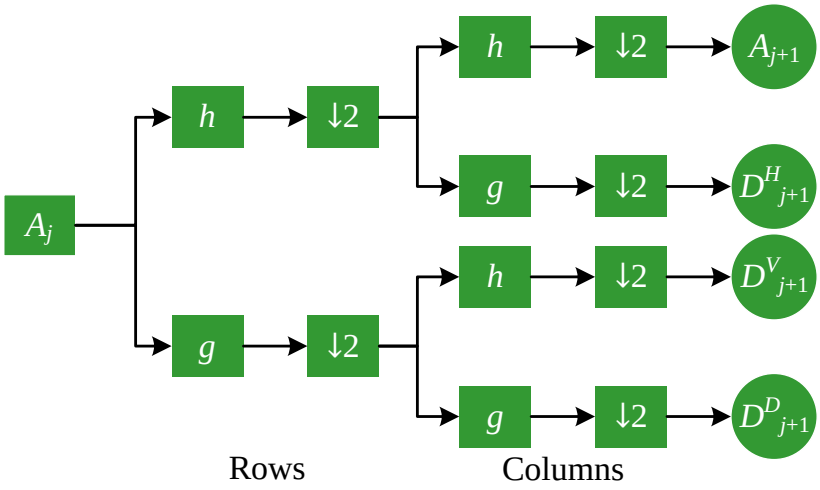

Fig. 1. An illustration of DWT, where A_j and A_{j+1} are the approximate coefficients at j and j+1 levels, h and g denote the high pass filtering and low pass filtering, D_{j+1}^H, D_{j+1}^V, and D_{j+1}^D refer to the detail coefficients along horizontal, vertical, and diagonal directions, respectively.

The selection of mother wavelet is critical for wavelet transform. There are many types of wavelet functions such as Daubechies, Harr, Coiflets, Symmlets, bi-orthogonal, Morlet, Mexican Hat, Meyer, and Butterworth [28]. The bi-orthogonal wavelets contain two sets of scale functions and wavelet functions for decomposition and reconstruction, which has promising amplitude and linear phase transmissions [28]. In this research, bi-orthogonal 6.8 wavelet [28] was used as the mother wavelet.

The DWT employs a dual channel filter to decompose the input surface topography data into multiple spatial bandwidths. The spatial bandwidths are related to the wavelet types and the decomposition levels. For surface texture characterisation, a suitable nesting index (a subset recommended value for filtering defined in ISO 25178-3 [30]) needs to be selected based on the primary surface. Selecting the nesting index for surface texture filtering is often task-specific, which is highly related to the applications. According to [24], the relationship between the decomposition level J and the nesting index N_i is described as:

$$N_i = \frac{2^J d}{F_c} \tag{7}$$

where F_c is the centre frequency of the wavelet and d is the sampling distance of the primary surface.

2.2 Probability-based new definitions of surface texture parameters

Surface texture parameters are important indicators for the functional performances of fatigue strength, friction behaviour, and optical interference and diffraction. According to ISO 25178-2 [12], there are height parameters, spacing parameters, hybrid parameters, functions and related parameters, and miscellaneous parameters in the field parameter definitions. In this research, five height parameters are evaluated - they are *Sa* (arithmetic mean height), *Sq* (root mean square height), *Sz* (maximum height), *Ssk* (skewness), and *Sku* (kurtosis). The height parameters are highly sensitive to the boundary effect. To reduce the boundary effect, a probability-based method named "95-99 rule" is proposed [8], which essentially uses a statistical portion (95% or 99%, according to different surface texture parameters as mentioned below) of the surface height data to calculate the surface texture parameters. The probability P for surface height $z(x, y)$ at α bilateral quantile is defined as:

$$P\{z(x,y) \le \lambda_1\} = P\{z(x,y) \ge \lambda_2\} = \frac{\alpha}{2} \quad \lambda_1 \le \lambda_2 \tag{8}$$

the boundary effect is illustrated by surface height $z(x, y)$ out of interval (λ_1, λ_2). Thus, surface texture parameters calculated with reduced boundary effect can be achieved by selecting a suitable interval. An example for 95% and 99% intervals under the Gaussian distribution is shown in Fig. 2, where the mean value is 0 and the standard deviation is 1 with 1000 data points. Here, *Sa*, *Sq, Ssk*, and *Sku* are calculated under 95% interval for their global descriptive characteristics and expressed as:

$$Sa = \frac{1}{MN} \sum_{i=1}^{M} \sum_{j=1}^{N} | z(x_i, y_j) | \tag{9}$$

$$Sq = \sqrt{\frac{1}{MN} \sum_{i=1}^{M} \sum_{j=1}^{N} z^2(x_i, y_j)} \tag{10}$$

$$Ssk = \frac{1}{MN \times Sq^3} \sum_{i=1}^{M} \sum_{j=1}^{N} z^3(x_i, y_j) \tag{11}$$

$$Sku = \frac{1}{MN \times Sq^4} \sum_{i=1}^{M} \sum_{j=1}^{N} z^4(x_i, y_j) \tag{12}$$

where M and N represent the sampling points in x and y directions. *Sz* is calculated under 99% interval for its local descriptive characteristics and it is expressed as:

$$Sz = Sp + Sv \tag{13}$$

where Sp is the maximum peak height and Sv is the minimum pit height.

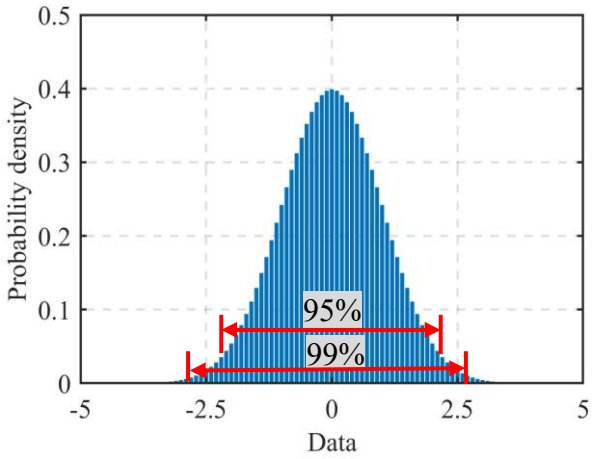

Fig. 2 An illustration for 95% and 99% intervals under a Gaussian distribution.

3. Experimental setup

Micro-lens array is a representative micro-structured surface, which is composed of a series of lenslet with the designed geometric features. During filtering the micro-lens array, its boundary effect would greatly occur for surface texture characterization. In experiments, a micro-structured surface (aspheric micro-lens array) was designed and the mathematical description of micro-aspheric lenslet was [31]:

$$Z(x,y) = \frac{S'CR_0^{\,2}}{4+4\sqrt{1-(1+K)C^2R_0^{\,2}}} - \frac{S'C\rho^2(x,y)}{4+4\sqrt{1-(1+K)C^2\rho^2(x,y)}} \tag{14}$$

where the shape parameter S' determines whether the micro-aspheric lenslet is concave (+1) or convex (-1), C is the curvature parameter, R_0 is the radius of each lenslet, K is the conic constant determining the eccentricity of the conic surface by K ($K < -1$: hyperboloid; $K = -1$: paraboloid; $-1 < K < 0$: ellipsoid; $K = 0$: sphere; and $K > 0$: oblate ellipsoid), and ρ is the radial operator. The parameters for the micro-aspheric lenslet are summarized in Table 1. Fig. 3 shows the design and simulation result for the micro-structured surface with 6 × 6 lenslets. Fig. 3(a) is the simulated topography, Fig. 3(b) is the simplified toolpath for clear observation which is generated using the equal angle discretisation method [32], and Fig. 3(c) presents the distribution of the lenslets at the six locations from the 1st lenslet (the closest distance to the spindle centre) to the 6th lenslet (the farthest distance to the spindle centre).

Table 1 Parameters of the micro-structured surface.

Shape parameter S'	1
Curvature C / mm^{-1}	0.8
Micro-asphere radius R_0 / mm	0.25
Conic constant K	-0.6
Height of each lenslet / μm	6.3
Distance between successive lenslets / mm	0.8

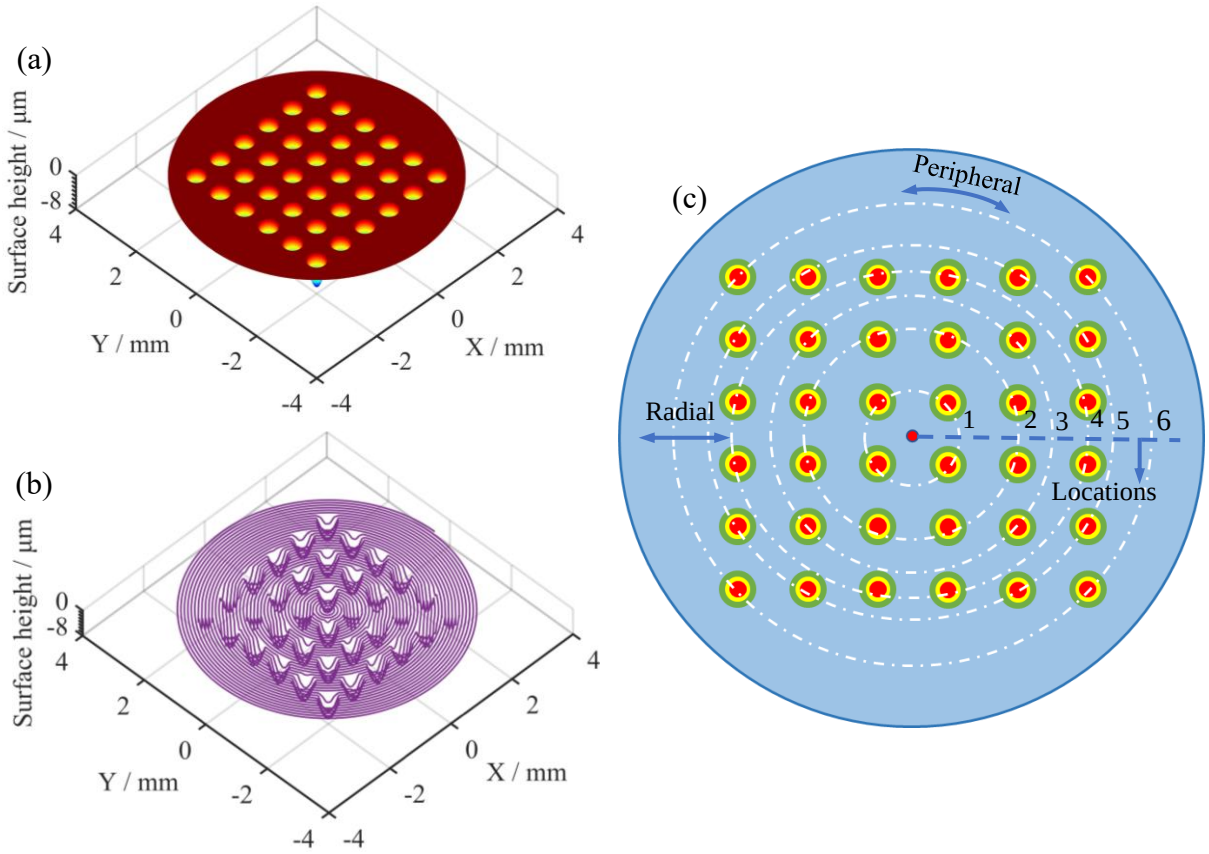

Fig. 3. Design and simulation result for the micro-structured surface: (a) the simulated surface topography, (b) the simplified toolpath, and (c) the distribution of lenslets.

The micro-lens array was machined by UPDT, in which the slow tool servo was applied to realize a large-scale fabrication with uniform surface generation. The UPDT experiment was carried out on a five-axis ultra-precision machine (Precitech Freeform TL) as shown in Fig. 4. The cutting parameters are selected in order to generate the required nanometric surface texture with little machining errors, considering the cutting performance under slow tool servo. The cutting conditions are shown in Table 2. Isotropic oxygen free copper was selected as the workpiece material and a natural single crystal diamond tool was adopted as the cutting tool. The measurement experiments

were performed on a white light interferometer (Bruker Contour GT-X) using stitching method to obtain a large surface topography with an area of 4.98 mm × 4.63 mm. The objective lens was 10× and the lateral sampling distance of the measurement result was 1.275 μm. Surface measurement by the white light interferometer can reach an ultra-high level of measurement accuracy. Its measurement uncertainty is at the vertical resolution of 0.05 nm and the repeatability of 0.01 nm (RMS). Potential errors can be attributed to the measurement errors such as the measurement noise and the surface residual dirt.

After measuring, the small-scale lateral components were removed from the measured surface by using the nesting index for the S-filter from the measuring instrument and, following this procedure, the primary surface was obtained [12]. The bi-orthogonal 6.8 wavelet was chosen for DWT, with the centre frequency F_c of 0.765 Hz and the sampling distance d of 1.275 μm. In line with ISO 25178-3 [30], the nesting indexes for the F-operator and L-filter were selected at 80 μm and 25 μm. According to Eq. (7), different spatial bandwidths of the surface topography data can be obtained by applying a six-level decomposition. The form, which is the underlying shape of micro-structured surface, is corresponding to the decomposed data with approximate coefficient at the 6th level (A_6), the S-F surface corresponds to a superposition of the detail coefficients from the 1st to the 6th level ($D_1 + D_2 + D_3 + D_4 + D_5 + D_6$), the S-L surface corresponds to the detail coefficients from the 1st to the 4th level ($D_1 + D_2 + D_3 + D_4$).

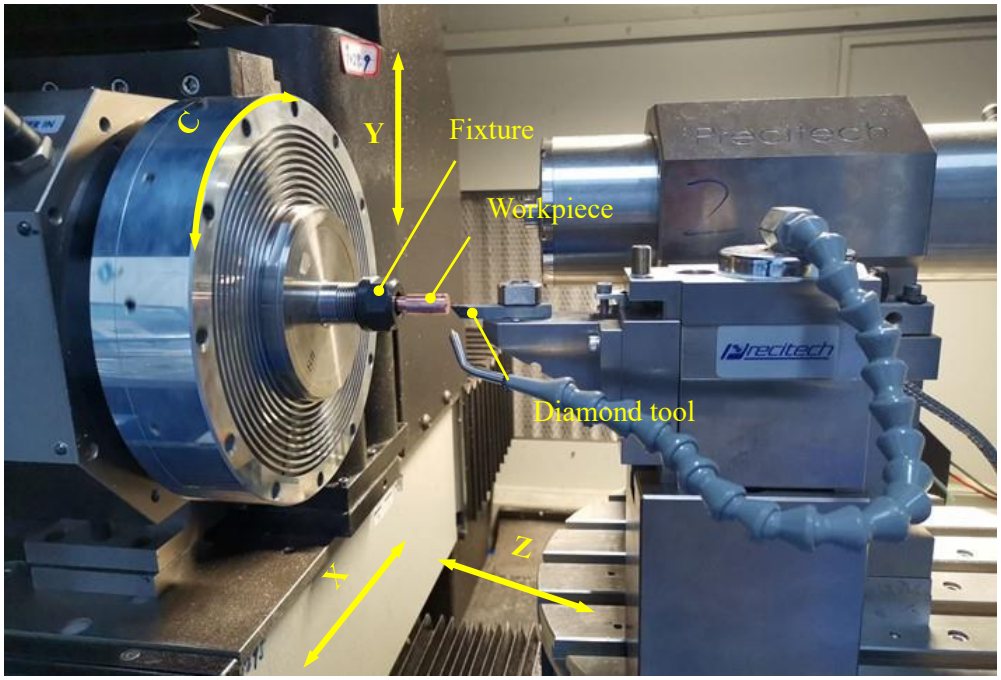

Fig. 4. UPDT of the micro-structured surface.

Table 2 Cutting conditions.

Workpiece material	Oxygen free copper
Sample aperture / mm	10
Tool nose radius / mm	0.3258
Tool rake angle / ◦	0
Front clearance angle / ◦	12
Spindle speed / rpm	25
Feedrate / mm min^{-1}	0.25

4. Results and discussion

4.1 Boundary effect during surface filtering

The topography of the machined micro-structured surface is a superposition of the high-frequency components that are caused by the material properties, servo vibration, the middle-frequency components (tool marks), and the low-frequency components (form), etc. Fig. 5 shows the result of surface filtering obtained by DWT with the proposed-above six-level decomposition. Fig. 5(a) shows the primary surface obtained by the white light interferometer fabricated by UPDT under the conditions of Table 2. The boundary areas of the micro-structures are well generated after UPDT. Fig. 5(b) shows its form component under the F-operator, which is corresponding to the decomposed data with the approximate coefficient at the 6^{th} level (A_6). It indicates that the boundary areas of the micro-structures, which contain the crucial feature of the geometrical information, are over-smoothed after surface filtering.

Fig. 5(c) shows the S-F surface by removing the form from the primary surface, which is a superposition of the detail coefficients from the 1^{st} to the 6^{th} level ($D_1 + D_2 + D_3 + D_4 + D_5 + D_6$). Fig. 5(d) represents the S-L surface, which corresponds to the detail coefficients from the 1^{st} to the 4^{th} level ($D_1 + D_2 + D_3 + D_4$), at the scale of the surface height ± 200 nm for a better visualisation of the detailed features. In Fig. 5(c) and (d), the boundary effect dramatically exists at the boundary areas of the micro-structures. It indicates that at the boundary areas the DWT would greatly lead to the filtering distortion with large amplitudes points [29]. Some burrs are obvious at the remote lenslets after surface filtering, which is influenced by the residual dirt after machining and measurement noise. Overall, the boundary effect would be produced significantly for the micro-structured surface by DWT filtering.

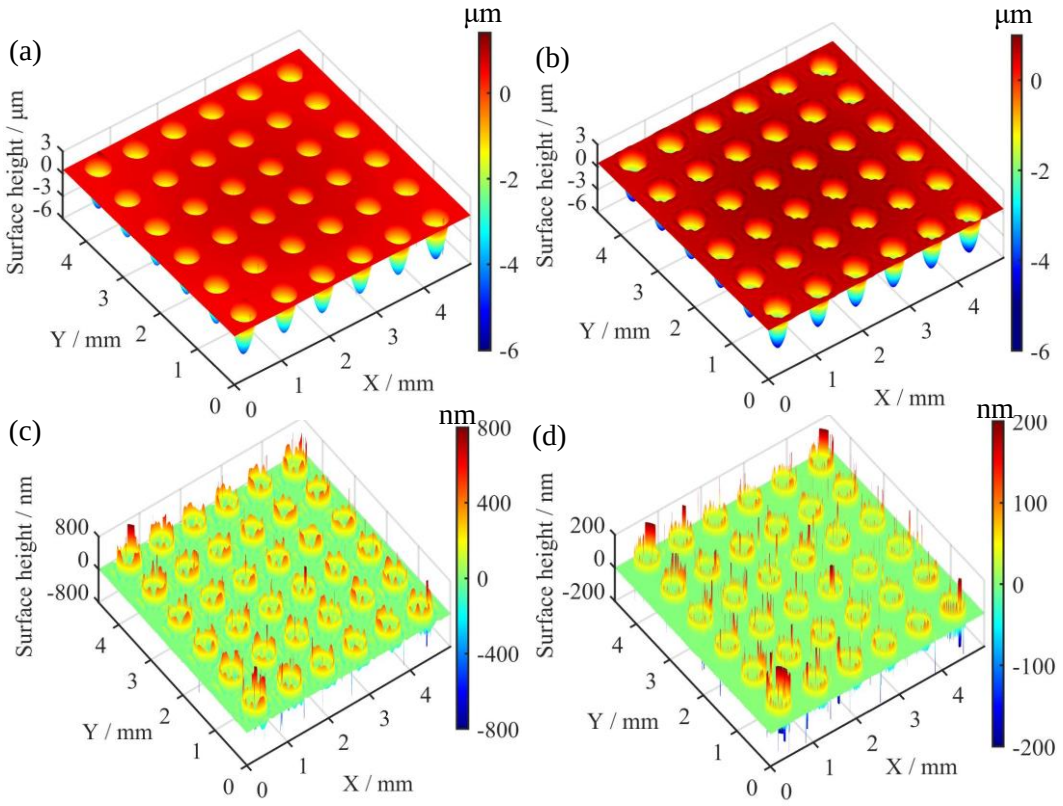

Fig. 5. Surface filtering by DWT: (a) primary surface, (b) form component (c) S-F surface, and (d) S-L surface.

4.2 Reduced boundary effect by the probability-based method

Based on the S-L surface in Fig. 5(d), one single lenslet was selected for the further surface analysis, as shown in Fig. 6. Fig. 6(a) is the primary surface of the selected lenslet. Fig. 6(b) shows the S-L surface under boundary effect by DWT filtering at the employed-above six-level decomposition, which corresponds to the detail coefficients from the 1st to the 4th level ($D_1 + D_2 + D_3 + D_4$). It shows that there exist the points with large amplitudes at the boundary of the lenslet. Fig. 6(c) shows the probability distribution of height datasets of Fig. 6(b). In Fig. 6(d), the boundary effect is reduced by the proposed probability-based method under the 95% interval. Moreover, the surface texture parameters are employed as the indicators for Fig. 6(b) with boundary effect under ISO 25178-2, and for Fig. 6(d) with reduced boundary effect under the proposed probability-based method. The results are shown in Table 3, where the differences refer to the ratios between the calculated deviations and the values with the reduced boundary effect. The values of the surface texture parameters were decreased by the proposed method, due to the fact that the boundary effect was reduced.

It is interesting to note that the behaviours of different surface texture parameters are different with the reduced boundary effect. For *Sa* and *Sq*, their values are reduced from 9.11 nm to 7.62 nm

(at the difference of 19.55%) and 11.53 nm to 9.16 nm (at the difference of 25.87%), respectively. For *Sz*, *Ssk*, and *Sku*, their values are significantly reduced from 330.98 nm to 73.26 nm (at the difference of 351.79%), 0.42 to 0.13 (at the difference of 223.08%), and 5.34 to 2.15 (at the difference of 148.37%), respectively. The differences of *Sa* and *Sq* are relatively small (about 20%), while the differences for *Sz*, *Ssk*, and *Sku* are relatively large (over 100%). It means that *Sz*, *Ssk*, and *Sku* are more sensitive to the boundary effect than *Sa* and *Sq*. This is because *Sz*, the maximum height of the probability distribution, is directly influenced by the large amplitude height. *Ssk* and *Sku* are the parameters with the higher order power of the probability distribution of height than *Sa* and *Sq*, since *Ssk* and *Sku* are the third-order/the fourth-order power of the probability distribution of height and *Sa* and *Sq* are the first-order/the second-order power of the probability distribution of height. Overall, the probability-based method is effective to reduce the boundary effect after surface filtering. *Sz*, *Ssk*, and *Sku* could be regarded as the more sensitive indicators for the boundary effect than *Sa* and *Sq*.

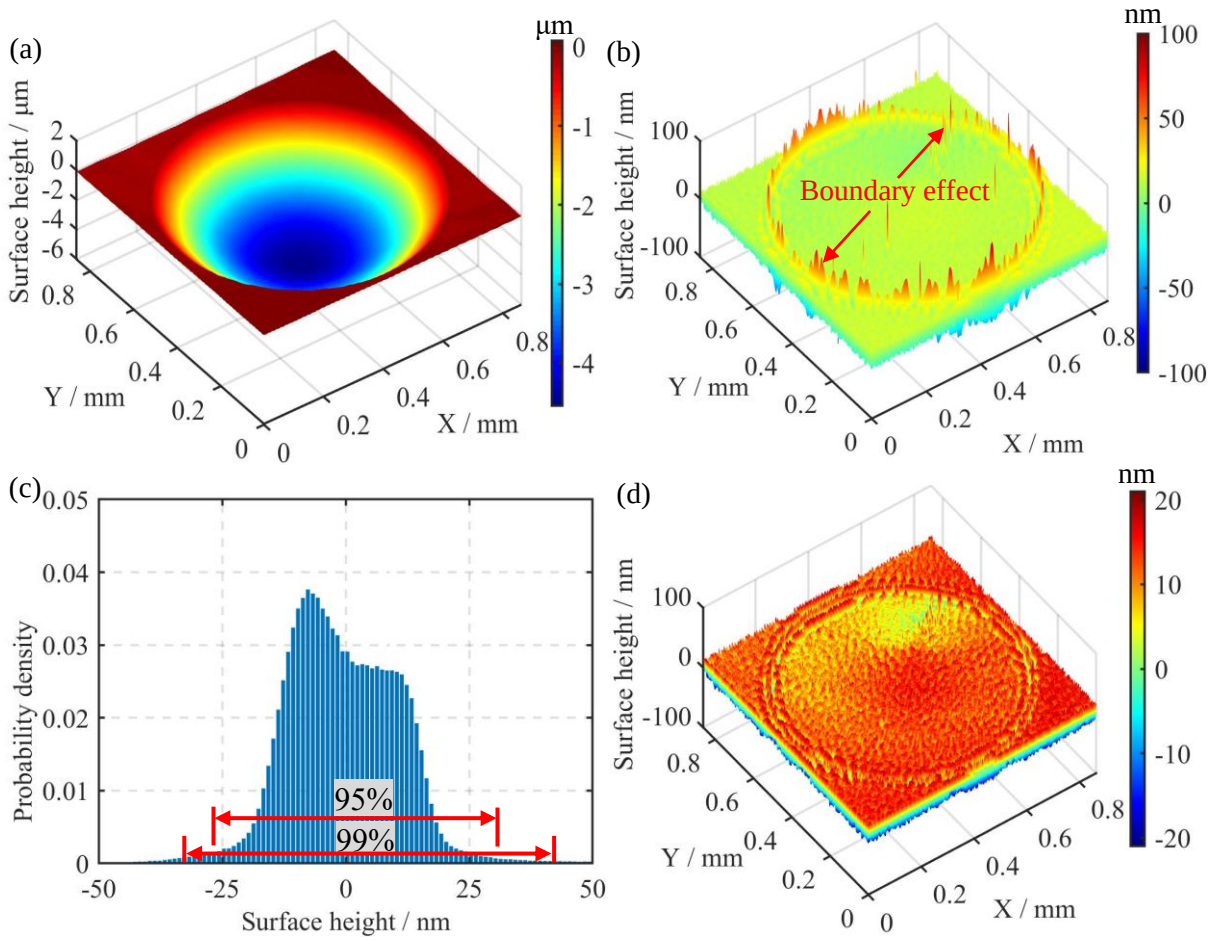

Fig. 6. Surface texture of the single lenslet: (a) primary surface, (b) S-L surface with boundary effect, (c) probability distribution of S-L surface datasets, and (d) S-L surface with reduced boundary effect.

Table 3 Surface texture parameters of the examined single lenslet.

	With boundary effect	With reduced boundary effect	Difference in %
Sa	9.11 nm	7.62 nm	19.55
Sq	11.53 nm	9.16 nm	25.87
Sz	330.98 nm	**73.26 nm**	**351.79**
Ssk	0.42	**0.13**	**223.08**
Sku	5.34	**2.15**	**148.37**

4.3 Surface texture characterisation

A comparison for all the lenslets (as shown in Fig. 5(a)) at the six locations from the 1st lenslet (the closest distance to the spindle centre) to the 6th lenslet (the farthest distance to the spindle centre) (as shown in Fig. 3(c)) with boundary effect and with reduced boundary effect has been conducted and the results are shown in Fig. 7. Fig. 7(a) (corresponding to Fig. 5(d)) shows the surface texture presented with boundary effect, there clearly existing many outliers at the boundary areas of the lenslets. Using the probability-based method, the outliers have been significantly reduced for all the lenslets, as shown in Fig. 7(b).

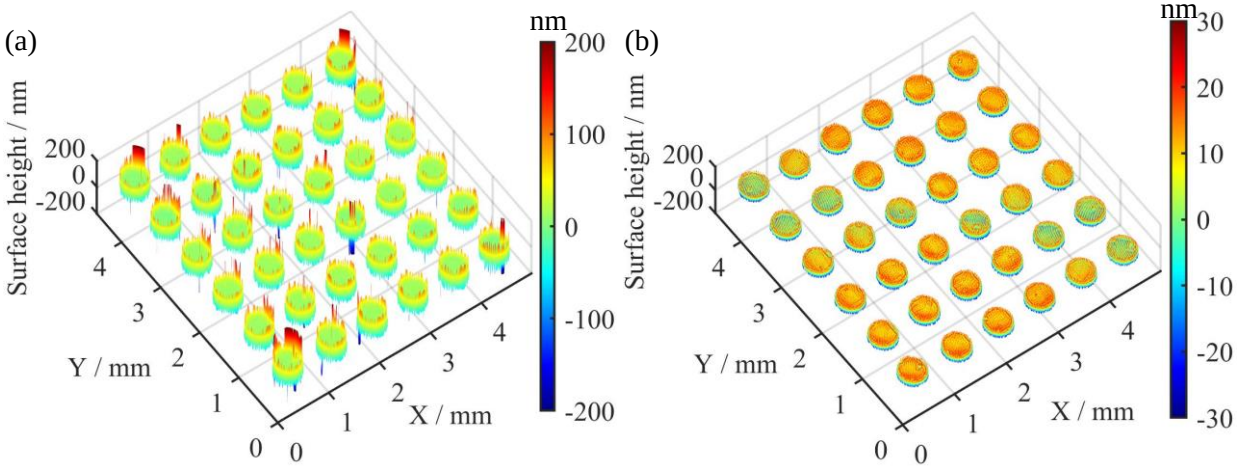

Fig. 7. S-L surface of lenslets at different locations: (a) with boundary effect and (b) with reduced boundary effect.

Surface texture parameters are evaluated for Fig. 7(a) with boundary effect according to ISO 25178-2, and for Fig. 7(b) with reduced boundary effect according to the proposed probability-based method. The calculated results are shown in Fig. 8 and the standard deviation σ of different surface texture parameters is listed in Table 4. In Fig. 8(a) and (b), *Sa* and *Sq*, describing the arithmetic mean

height and the root mean square height of the surface texture, decrease with the reduced boundary effect and the trend is consistent for all the lenslets. In Fig. 8(c) - (e), *Sz*, *Ssk*, and *Sku* are fluctuating with large deviations under boundary effect. It also means that *Sz*, *Ssk*, and *Sku* are more sensitive to the boundary effect than *Sa* and *Sq*.

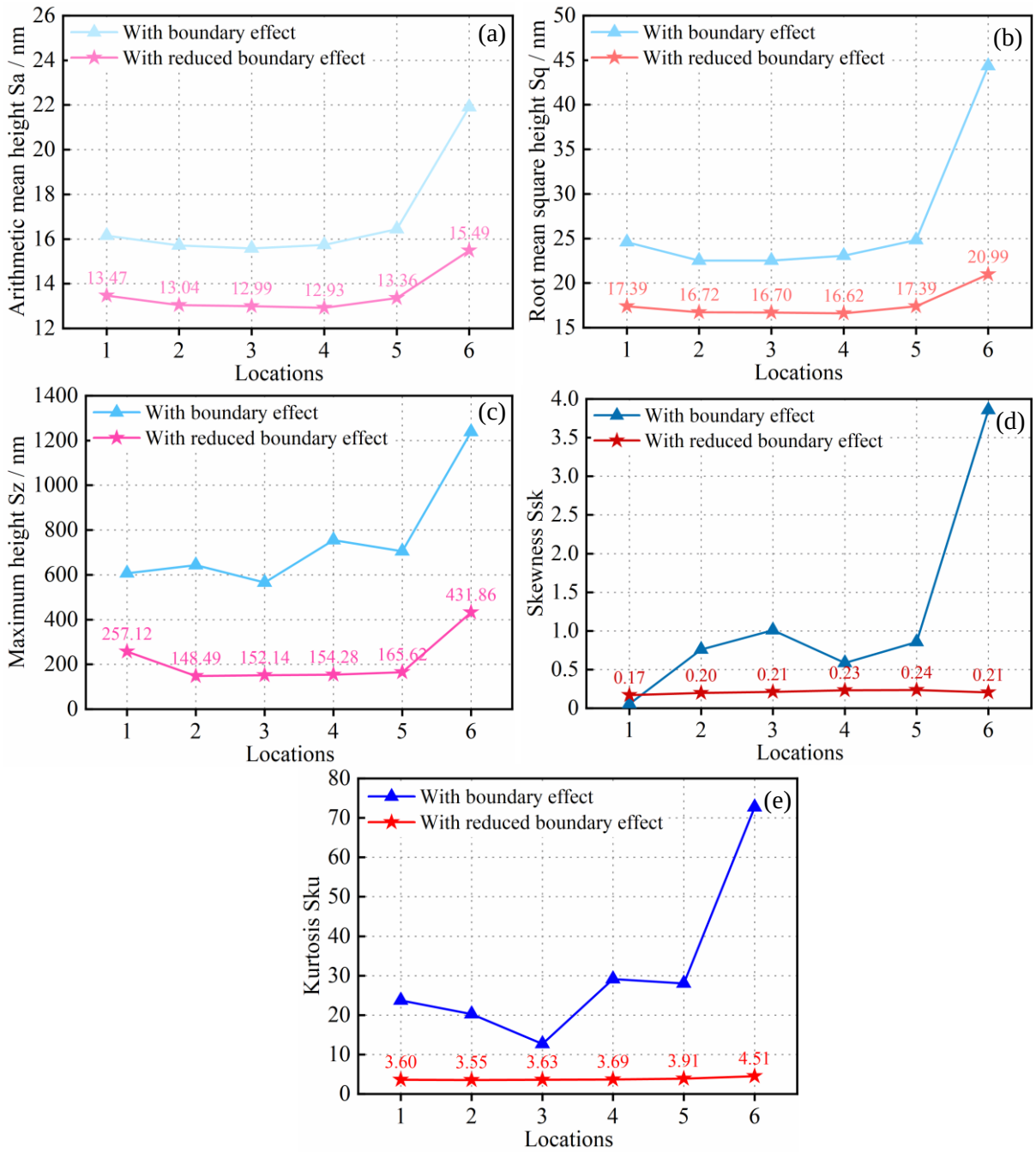

Fig. 8. Surface texture parameters calculated with boundary effect and with reduced boundary effect: (a) *Sa*, (b) *Sq*, (c) *Sz*, (d) *Ssk*, and (e) *Sku*.

Using the proposed probability-based method, their values have been significantly reduced, and

become more stable (without significant fluctuations), as shown in Table 4. *Sz*, the sum of the maximum peak height and the minimum pit height, is significantly decreased. *Ssk* (the asymmetry of the height distribution) is positive. *Sku* (a measure of randomness of the surface texture) is greater than 3. It means that the nanometric surface texture is mainly dominated by the spiky-shaped texture such as material pile-up and tool marks. Overall, using the probability-based method for nanometric surface texture characterisation, more reliable results are obtained for the micro-structured surface.

Table 4 Standard deviation of surface texture parameters for all lenslets.

Standard deviation σ	*Sa*	*Sq*	*Sz*	*Ssk*	*Sku*
With boundary effect	2.46 nm	8.57 nm	247.54 nm	1.35	21.23
With reduced boundary effect	0.97 nm	1.68 nm	112.46 nm	0.02	0.36

5. Conclusions

Ultra-precision diamond turning (UPDT) offers a reliable solution for manufacturing of micro-structured surfaces with nanometric surface texture. Commercial surface measurement instruments such as white light interferometers are able to provide accurate surface measurement results. However, the boundary effect significantly affects the nanometric surface texture characterisation of micro-structured surfaces when applying topography filtering. In this study, a new method was proposed with applying discrete wavelet transform (DWT) to extract the surface texture from the primary surface and a probability-based approach to reduce the boundary effect of micro-structured surfaces. The main conclusions are drawn as follows:

(1) Nanometric surface texture can be separated from the micro-structured by DWT filtering, but the boundary effect dramatically occurs at the boundary of micro-structures and significantly affects their surface texture characterisation.

(2) ISO surface texture parameters are greatly influenced by the boundary effect during surface filtering. Especially, *Sz*, *Ssk*, and *Sku* were more sensitive to the boundary effect than *Sa* and *Sq*, since *Sz* is the maximum height of the probability distribution, *Ssk* and *Sku* are the parameters with the higher order power of the probability distribution of height than *Sa* and *Sq*.

(3) Using the proposed probability-based method, the boundary effect can be efficiently reduced for the micro-structured surfaces. Significantly, a more convincing nanometric surface texture characterisation can be achieved for the micro-structured surfaces.

The study is beneficial for the development of nanomanufacturing and nanometrology. However, surface texture parameters are not systematically discussed because only the height parameters of ISO 25178-2 are characterized. Moreover, the relationship between the functional performance and the nanometric surface texture of micro-structured surfaces is not further studied. Future work will be focused on the above limitation and applying the proposed method for different types of micro-structured surfaces.

Credit Author Statement

Pan Guo: Conceptualization, Methodology, Software, Investigation, Data curation, Writing - original draft. **Mingyu Liu**: Investigation, Writing - review & editing. **Bowen Zhang**: Software, Investigation. **Jintao Li**: Software, Investigation. **Zhiwen Xiong**: Investigation, Formal analysis, Writing - review & editing. **Samanta Piano:** Writing - review & editing. **Shaojian Zhang**: Resources, Validation, Writing - review & editing, Supervision, Project administration.

Acknowledgments

This work was supported by the National Natural Science Foundation of China [Grant no. 51405217] and the European Metrology Programme for Innovation and Research [TracOptic, 20IND07].

Declaration of conflicting interests

The author(s) declared no potential conflicts of interest with respect to the research, authorship and/or publication of this article.

References

[1] Brinksmeier, E., Gläbe, R., Schönemann, L. (2012). Review on diamond-machining processes for the generation of functional surface structures. *CIRP Journal of Manufacturing Science and Technology*, 5(1), 1-7.

[2] Zhang, X., Liu, Q., Zhou, X., Lin, C. (2015). Determining issues in optimal turning of micro-structured functional surfaces. *The International Journal of Advanced Manufacturing Technology*, 81(1), 387-396.

[3] Kong, L.B., Cheung, C.F. (2011). Design, fabrication and measurement of ultra-precision micro-structured freeform surfaces. *Computers & Industrial Engineering*, 61(1), 216-225.

[4] Zhu, Z., Zhou, X., Luo, D., Liu, Q. (2013). Development of pseudo-random diamond turning method for fabricating freeform optics with scattering homogenization. *Optics Express*, 21(23), 28469-28482.

[5] Zhang, S., Zhou, Y., Zhang, H., Xiong, Z., To, S. (2019). Advances in ultra-precision machining of micro-structured functional surfaces and their typical applications. *International Journal of Machine Tools and Manufacture*, 142, 16-41.

[6] Hatefi, S., Abou-El-Hossein, K. (2020). Review of single-point diamond turning process in terms of ultra-precision optical surface roughness. *The International Journal of Advanced Manufacturing Technology*, 106(5), 2167-2187.

[7] Whitehouse, D.J. (2010). Handbook of Surface and Nanometrology. CRC Press.

[8] Zhang, S.J., To, S., Wang, S.J., Zhang, G.Q. (2016). A new representation with probability distribution for nanometric surface roughness in ultra-precision machining. *Precision Engineering*, 45, 445-449.

[9] Nieslony, P., Krolczyk, G. M., Wojciechowski, S., Chudy, R., Zak, K., & Maruda, R. W. (2018). Surface quality and topographic inspection of variable compliance part after precise turning. *Applied Surface Science*, 434, 91-101.

[10] Pawlus, P., Reizer, R., Wieczorowski, M., & Krolczyk, G. (2020). Material ratio curve as information on the state of surface topography—A review. *Precision Engineering*, 65, 240-258.

[11] Gong, Y., Xu, J., & Buchanan, R. C. (2018). Surface roughness: A review of its measurement at micro-/nano-scale. *Physical Sciences Reviews*, 3(1).

[12] ISO 25178-2:2012. Geometrical Product Specifications (GPS) — Surface Texture: Areal — Part 2: Terms, Definitions and Surface Texture Parameters.

[13] Nieslony, P., Krolczyk, G. M., Zak, K., Maruda, R. W., & Legutko, S. (2017). Comparative assessment of the mechanical and electromagnetic surfaces of explosively clad Ti–steel plates after drilling process. *Precision Engineering*, 47, 104-110.

[14] Pomberger, S., Stoschka, M., & Leitner, M. (2019). Cast surface texture characterisation via areal roughness. *Precision Engineering*, 60, 465-481.

[15] Jiang, X.J., Whitehouse, D.J. (2012). Technological shifts in surface metrology. *CIRP Annals*, 61(2), 815-836.

[16] Yang, H., Zhang, X., Zhang, H., He, X., Xiao, H., & Xu, M. (2017). Feature-preserving filtering for micro-structured surfaces using combined sparse regularizers. *Measurement*, 104, 278-286.

[17] Lou, S., Tang, D., Zeng, W., Zhang, T., Gao, F., Muhamedsalih, H., & Scott, P. J. (2020).

Application of clustering filter for noise and outlier suppression in optical measurement of structured surfaces. *IEEE Transactions on Instrumentation and Measurement*, 69(9), 6509-6517.

[18] Li, H., Cheung, C. F., Jiang, X. Q., Lee, W. B., & To, S. (2006). A novel robust Gaussian filtering method for the characterization of surface generation in ultra-precision machining. *Precision Engineering*, 30(4), 421-430.

[19] Zeng, W., Jiang, X., & Scott, P. (2011). A generalised linear and nonlinear spline filter. *Wear*, 271(3-4), 544-547.

[20] Liu, M.Y., Cheung, C.F., Feng, X., Ho, L.T., Yang, S.M. (2019). Gaussian process machine learning-based surface extrapolation method for improvement of the edge effect in surface filtering. *Measurement*, 137, 214-224.

[21] Abdul-Rahman, H.S., Jiang, X.J., Scott, P.J. (2013). Freeform surface filtering using the lifting wavelet transform. *Precision Engineering*, 37(1), 187-202.

[22] Gogolewski, D. (2021). Fractional spline wavelets within the surface texture analysis. *Measurement*, 179, 109435.

[23] Brown, C.A., Hansen, H.N., Jiang, X. J., Blateyron, F., Berglund, J., Senin, N., Zahouani, E.H. (2018). Multiscale analyses and characterizations of surface topographies. *CIRP Annals*, 67(2), 839-862.

[24] Zou, Y., Li, Y., Kaestner, M., Reithmeier, E. (2016). Low-coherence interferometry based roughness measurement on turbine blade surfaces using wavelet analysis. *Optics and Lasers in Engineering*, 82, 113-121.

[25] Wang, X., Shi, T., Liao, G., Zhang, Y., Hong, Y., Chen, K. (2017). Using wavelet packet transform for surface roughness evaluation and texture extraction. *Sensors*, 17(4), 933.

[26] Ali, J.M., Jailani, H.S., Murugan, M. (2020). Surface roughness evaluation of electrical discharge machined surfaces using wavelet transform of speckle line images. *Measurement*, 149, 107029.

[27] Wang, H.X., Zong, W.J., Sun, T., Liu, Q. (2010). Modification of three dimensional topography of the machined KDP crystal surface using wavelet analysis method. *Applied Surface Science*, 256(16), 5061-5068.

[28] Fu, S., Muralikrishnan, B., Raja, J. (2003). Engineering surface analysis with different wavelet bases. *Journal of Manufacturing Science and Engineering*, 125(4), 844-852.

[29] Gogolewski, D. (2020). Influence of the edge effect on the wavelet analysis process. *Measurement*, 152, 107314.

[30] ISO 25178 (2012) Geometric Product Specifications (GPS) — Surface Texture: Areal — Part 3:

Specification Operators.

[31] Zhu, Z., To, S., Zhang, S. (2015). Large-scale fabrication of micro-lens array by novel end-fly-cutting-servo diamond machining. *Optics Express*, 23(16), 20593-20604.

[32] Liu, Y., Qiao, Z., Qu, D., Wu, Y., Xue, J., Li, D., & Wang, B. (2018). Experimental investigation on form error for slow tool servo diamond turning of micro lens arrays on the roller mold. *Material*s, 11(10), 1816.